water

MDPI

*Article*

# Sentinel-1 and Sentinel-2 Data to Detect Irrigation Events: Riaza Irrigation District (Spain) Case Study

**Anna Balenzano [1,*], Giuseppe Satalino [1], Francesco Paolo Lovergine [1], Annarita D'Addabbo [1], Davide Palmisano [1], Riccardo Grassi [1], Ozlem Ozalp [1], Francesco Mattia [1], David Nafría García [2] and Vanessa Paredes Gómez [2,*]**

[1] Institute for Electromagnetic Sensing of the Environment (IREA), National Research Council of Italy (CNR), 70126 Bari, Italy
[2] Instituto Tecnológico Agrario de Castilla y León (ITACyL), 47071 Valladolid, Spain
* Correspondence: balenzano.a@irea.cnr.it (A.B.); pargomva@itacyl.es (V.P.G.)

**Abstract:** This paper investigates the use of high resolution (~100 m) surface soil moisture (SSM) maps to detect irrigation occurrences, in time and space. The SSM maps have been derived from time series of Copernicus Sentinel-1 (S-1) and Sentinel-2 (S-2) observations. The analysis focused on the Riaza irrigation district in the Castilla y León region (Spain), where detailed information on land use, irrigation scheduling, water withdrawal, meteorology and parcel borders is available from 2017 to 2021. The well-documented data basis has supported a solid characterization of the sources of uncertainties affecting the use of SSM to map and monitor irrigation events. The main factors affecting the irrigation detection are meteo-climatic condition, crop type, water supply and spatial and temporal resolution of Earth observation data. Results indicate that approximately three-quarters of the fields irrigated within three days of the S-1 acquisition can be detected. The specific contribution of SSM to irrigation monitoring consists of (i) an early detection, well before vegetation indexes can even detect the presence of a crop, and (ii) the identification of the irrigation event in time, which remains unfeasible for vegetation indexes. Therefore, SSM can integrate vegetation indexes to resolve the irrigation occurrences in time and space.

**Keywords:** Sentinel-1; Sentinel-2; high resolution soil moisture; irrigation event detection; uncertainties



**Citation:** Balenzano, A.; Satalino, G.; Lovergine, F.P.; D'Addabbo, A.; Palmisano, D.; Grassi, R.; Ozalp, O.; Mattia, F.; Nafría García, D.; Paredes Gómez, V. Sentinel-1 and Sentinel-2 Data to Detect Irrigation Events: Riaza Irrigation District (Spain) Case Study. *Water* **2022**, *14*, 3046. https://doi.org/10.3390/w14193046

Academic Editors: Sara Álvarez and Cristina Romero-Trigueros

Received: 30 July 2022
Accepted: 22 September 2022
Published: 27 September 2022



## 1. Introduction

Irrigated agriculture absorbs large volumes of freshwater and highly influences crop production and quality, especially in arid and semi-arid regions, such as the Mediterranean basin, where irrigated agriculture represents 65% of total water taken [1,2]. The increase in evaporative demand due to climate change projected over these areas [3] will likely lead to a significant reduction in water availability, heightened by the consequent increase in irrigation needed to preserve crop yield volumes [4,5]. The result may not be sustainable and suggests a vicious cycle from water scarcity to food insecurity and social fragility [6]. Specific responses to mitigate, adapt and cope with the effects of such a scenario include integrated water resources management and increased monitoring [7,8]. For instance, the space and time distribution of irrigated areas is a necessary input to simulate the water withdrawal that is crucial information for effective water management [9]. Moreover, a recent study [10] demonstrated a strong and linear relationship between the extent of irrigated areas and irrigation water withdrawal, evaluated at continental and national scales over Europe, Africa, the Americas and Asia. Under these circumstances, a reliable estimate of irrigated areas can be the key to more informed management of water resources. However, current estimates of the extent of irrigated croplands at global and regional scales are highly uncertain [11]. In addition, significant differences between statistics and model predictions exist (e.g., [12]). The implication is hampering an effective water governance

and understanding of the impact of irrigation on the hydrologic cycle. Puy et al. [13] argued that a step forward would be acknowledging and characterizing the sources of uncertainties and their impact. The envisaged perspective is integrating uncertainties into advanced models of water management that may serve credible and effective governance of water resources.

This study embraces such a vision and aims at further characterizing uncertainties in estimating irrigated areas. The adopted method combines Synthetic Aperture Radar (SAR) and optical Earth observation (EO) data.

In past studies, a great deal of work has been carried out demonstrating the potential of optical, thermal and microwave data to detect irrigated areas (for recent reviews, see, e.g., [14–17]). Historically, the most used approach exploits vegetation indexes, such as the Normalized Difference Vegetation Index (NDVI), derived solely from optical data (e.g., [18]). Its main limitation is that reliable observations require clear sky conditions. Additionally, vegetation indices are generally sensitive to the greenness of the canopy and, therefore, there is an indirect dependence on the water supply. As a consequence, irrigation maps derived from optical data usually come late in the growing season and only for crops with high water requirements. For instance, it is very challenging for EO optical data to identify fields for which irrigation remains supplemental (e.g., wheat). In terms of uncertainties, the approach is affected by the threshold levels adopted for the vegetation indexes [18], by the spatial resolution of the EO products (generally, the coarser the resolution the higher the uncertainty [19,20]) and by meteorology, e.g., temperature and precipitation [21].

More recently, the contribution of microwave EO data for irrigation detection has also been investigated. The rationale is that microwave EO data show a high sensitivity to surface soil moisture (SSM) content and there exists a correlation between SSM and the application of irrigation water. In this vein, the availability of operational SSM products derived from spaceborne radiometers and/or scatterometers (e.g., Soil Moisture and Ocean Salinity (SMOS) mission of the European Space Agency (ESA), the Soil Moisture Active Passive (SMAP) mission of the National Aeronautics and Space Administration (NASA) and the Advanced SCATterometer (ASCAT) system aboard the Meteorological Operational (MetOp) platform of the European Organization for the Exploitation of Meteorological Satellites (EUMETSAT)) has stimulated their use to assess the potential to detect irrigated areas [22–24]. An outcome of these studies is that the coarse resolution of ASCAT, SMOS and SMAP SSM products (~25 km) is a major limitation to monitoring soil moisture changes due to irrigation management that often take place at scales of a few hundred meters [9].

The launch of the Sentinel-1 (S-1) constellation of the European Union (EU) Copernicus program, performing C-band SAR high space (~10 m) and time (six-day exact revisit) resolution observations with a sustained and systematic acquisition plan, has mobilized new energies towards the use of SAR data for SSM retrieval at high resolution (100–1000 m). Various SSM products covering large areas have been proposed and assessed by several teams, e.g., [25–27]. Subsequently, the same products or their evolutions have been used to understand the potential of SAR data to map irrigated areas (e.g., [28–32]). Promising results have been obtained in segmenting or classifying irrigated areas. However, the causes contributing to the uncertainty of the results are less investigated.

This study leverages extensive information on irrigation management in the irrigation district of Riaza, in the Castilla y León region (Spain). Parcel borders, irrigation scheduling, irrigation water withdrawal, planted crops, meteorology, etc. are the data made available for more than 700 fields monitored over five years (2017–2021) by ITACyL, part of Castilla y León (Spain) Common Agricultural Policy Paying Agency. The ground information serves to assess the impact of spatial and temporal resolution of time series of SAR and multi-spectral data, acquired by S-1 and Sentinel-2 (S-2) systems, on the detection of irrigated agricultural fields. Moreover, the role of precipitation and vegetation cover is investigated. The overarching objective is to trace the causes of incertitude in mapping irrigated areas using EO SSM data at high resolution and determine their impact on the retrieval of the

spatial and temporal extent of the irrigation occurrences. The occurrence of irrigation is called an irrigation event. Indeed, the integrative use of high resolution microwave and optical data enables the estimation of the location and extent of irrigated fields, but also the time interval in which the events took place. This can be valuable information for irrigation management in various instances. It can, for example, support the detection of supplemental irrigation that is expected to significantly increase for rain-fed crops, such as wheat, to better cope with water scarcity [11,33]. To date, tracking supplemental irrigation at a large scale solely using optical data is quite challenging. A second possible benefit is the detection of irrigated areas early in the season, i.e., before the emergence of the plants. Such information can enable timely estimates of irrigated areas' extent.

In the next section, the method adopted in the study is described. In addition, the data basis analyzed is illustrated. Then, the obtained results are presented and discussed.

## 2. Materials and Methods

The value of the high resolution (~100 m) SSM maps to identify irrigated areas relies on the observation that, in a time interval, irrigated fields show an SSM level higher than non-irrigated fields. The "Soil MOisture retrieval from multi-temporal SAR data" (SMOSAR) code, developed in the European Space Agency (ESA) SEOM Exploit-S-1 project (https://seom.esa.int/page_project034.php, accessed on 26 September 2022) and further improved within the EU SARAGRI project (http://sensagri.eu, accessed on 26 September 2022), is used to obtain the SSM fields at a regional scale (e.g., [34,35]). Currently, SMOSAR SSM output can be either at ~1000 m or ~100 m resolution every 6–12 days. The input for the first case consists of time series of S-1 alone. Conversely, both S-1 and S-2 time series are required to obtain SSM maps at the highest resolution.

In the next subsections, first, the data basis of the study is illustrated. The study area, ground and EO data are introduced. Subsequently, SMOSAR is described and the properties of SSM for detecting irrigated areas with respect to NDVI are discussed. The issue of the spatial resolution is also addressed. Finally, the SSM contrast, i.e., the ratio between the SSM of irrigated and non-irrigated fields, is defined and adopted in the analysis. Indeed, a relative measure of SSM is needed because the absolute SSM value is highly influenced by the characteristics of the site, e.g., climate, orography, soil properties, agriculture management, etc. For these reasons, the contrast between the SSM levels of irrigated and non-irrigated fields is a more robust metric, indicating whether or not a field is significantly dryer/wetter than the surrounding area.

### 2.1. Test Site and Ground Data

The Riaza irrigation district in the Castilla y León region (Spain) comprises 5232 ha along an approximately 45 km canal that flows parallel to the Duero River. The Riaza area is composed of 991 fields, with a size ranging from 0.04 ha to 65.0 ha (2.6 ha on average). Meteorological data over the area are acquired by the station VA07 of the national agrometeorological network included in the Inforiego irrigation advice service (https://www.inforiego.org/opencms/opencms, accessed on 26 September 2022). The meteorological station measures air temperature and humidity, wind speed and direction, solar radiation and reference evapotranspiration.

The irrigation district is fully automated and scheduled. A central database records all the irrigation events from all the hydrants connected to the system. Over the Riaza area, the irrigation technique is mostly based on sprinklers and the consumption of water is well documented. From 2017 to 2021 and for each agricultural field, in situ data include information on crop type, the start and the end time of each scheduled water supply and the amount of water consumption. In order to translate information from hydrant level to field level, a geographic information system (GIS), based on the Land Parcel Identification System, has been built.

Figure 1 shows the location of the Riaza irrigation district and the parcel borders overlayered on the S-2 NDVI map on 30 April 2019, where the winter crops are visible in

medium-dark green. The red point represents the VA07 meteorological station. Winter (e.g., wheat and barley) and summer (e.g., sugar beet and maize) crops, together with some permanent crops, are cultivated.

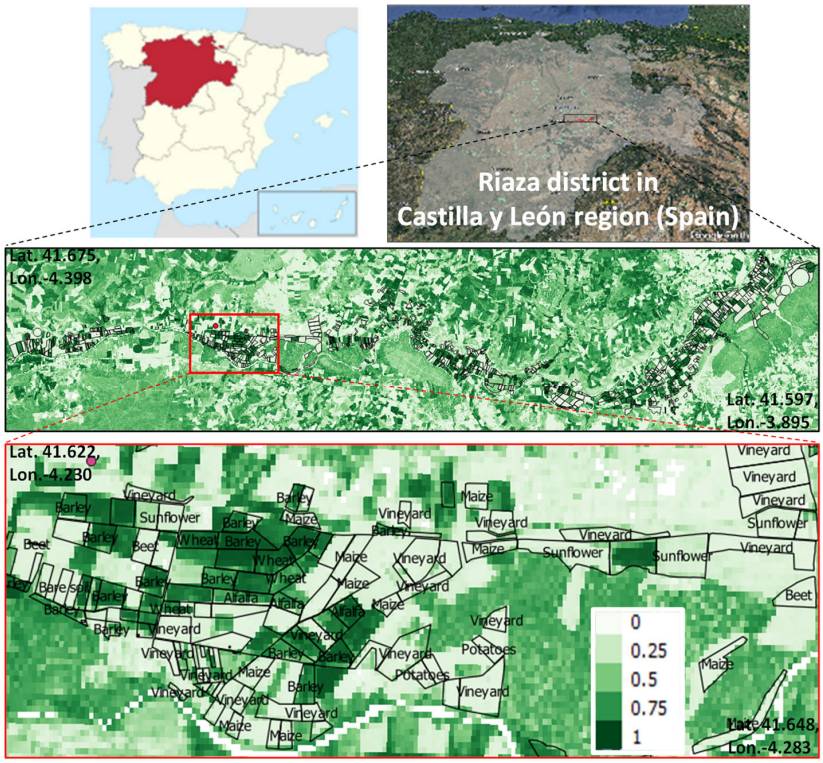


**Figure 1. Top panel**: Castilla y León region in Spain and the Riaza irrigation district location. **Middle panel**: zoomed-in view of the black rectangle with parcel borders overlayered on the S-2 NDVI on 30 April 2019. Red point indicates the VA07 Inforiego meteorological station. **Bottom panel**: zoomed-in view of the red rectangle with crop type information. Geographic coordinates of the corners are reported.

In the data analysis, fields larger than 2 ha and with homogeneous cover for more than 50% of their size have been considered. For the scope of this paper, a field is defined as irrigated if and only if it received a water supply 5 to 0 days before the corresponding S-1 passage. Six days is the exact revisit time of the S-1 constellation. From 2017 to 2021, 5270 irrigation events were registered over 751 fields cultivated with the main seasonal crops, i.e., wheat, barley, maize, sugar beet, sunflower, potatoes, alfalfa and garlic. Figure 2 (left panel) reports the percentages of crop types cultivated. In the right panel, the percentage of irrigation events, according to the above definition, is reported. The percentage is with respect to the total number of events recorded in the farm log.

The seasonal crops selected for the statistical analysis are wheat, barley and maize, as they are the main crops in terms of the number of fields and irrigation events. Indeed, they represent 68% of the total fields with 62% of the total irrigation events. This selection is also supported by the fact that wheat/barley and maize present a different canopy structure which affects their response to the radar signal at the C-band. In fact, for agricultural areas, the interaction between the radar signal and the crop canopy is dominated by scattering mechanisms that significantly change with plant architecture and fresh biomass. The latter is in turn strongly related to the phenological cycle and ultimately to the period in the growing season (i.e., the day of the year, DoY). At the C-band, two extreme classes of seasonal crops can be identified based on their radar response [36]. The first class includes crops for which the volume scattering mechanism is dominant (e.g., sugar beet, potatoes and maize). In these cases, at the mature stage, the radar backscatter is poorly correlated with the in situ SSM observations. Conversely, the second class includes crops, such as

wheat, barley and oat, for which a good sensitivity of the C-band radar signal to SSM exists throughout the growing season. Indeed, they are dominated by surface scattering [37].

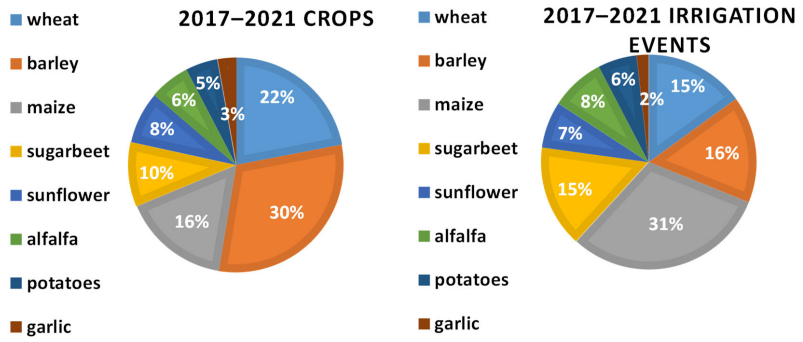


**Figure 2. Left panel**: percentage of main crops with an extent larger than 2 ha irrigated from 2017 to 2021. **Right panel**: percentage of irrigation events per crop (**right panel**).

The selected crops also differ in their growing season. Figure 3 (top panel) shows the temporal behavior of the S-2 NDVI averaged over all the fields of the Riaza district, cultivated with wheat and maize in 2019. Wheat is a winter crop, which reaches its peak at the end of April or the beginning of May, while maize is a summer crop. Its mature phase is between the beginning of July and the end of August. For wheat, the senescence begins in June, while for maize in September. Regarding the inter-annual variability in the growing season, Figure 3 (bottom panel) shows, as an example, the temporal behavior of the S-2 NDVI averaged over all wheat and barley crops from 2017 to 2021. The shaded area refers to the related standard deviation. As the inter-annual variability is less than 0.16 over the growing season, it is evident that the crop growth follows a fairly similar behavior from year to year. Therefore, the multi-year data set has been considered as unique per crop.

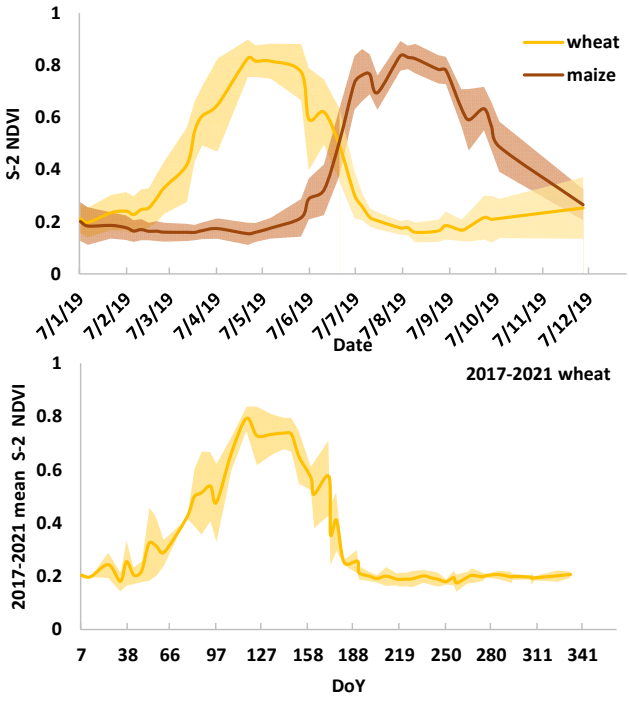


**Figure 3. Top panel**: NDVI derived from S-2 data over all the wheat and maize fields of the Riaza district in 2019. The shaded area represents the inter-field variability. **Bottom panel**: NDVI derived from S-2 data and averaged over all the winter wheat and barley fields of the Riaza district from 2017 to 2021. The shaded area represents the inter-annual variability. DoY stands for day of the year.

Concerning the irrigation practices, both winter and summer crops are irrigated, though with different strategies. Figure 4 shows the temporal series of the irrigation events registered over the wheat and barley (red) and maize (green) fields irrigated 5 to 0 days before the S-1 passages from 2017 to 2021. The red and green shaded areas represent the corresponding total extent of the irrigated fields. The monthly precipitation rate is also reported in light blue. In general, wheat and barley are mostly irrigated from early April to June and maize from June to September. For maize, irrigation is quasi-continuous, while for winter wheat/barley, the irrigation, in most cases, is supplemental. Moreover, the number of irrigated fields significantly differs from 2017 to 2021. This is due to the largely variable meteorological conditions, which drive the irrigation scheduling. For example, April 2017 was unusually dry, therefore winter and barley fields were abundantly irrigated, while, on the other extreme, the whole spring of 2018 was very wet and winter crops were sparsely irrigated. This means that the number of irrigated events and irrigated area, in the case of supplemental irrigation, are extremely variable from year to year and month to month. It may also happen to observe only one event for some wheat/barley fields. Conversely, the number of maize irrigated fields and related irrigated area are more stable per year and month. A quantitative analysis of the temporal trend of irrigation areas will be addressed in a future study.

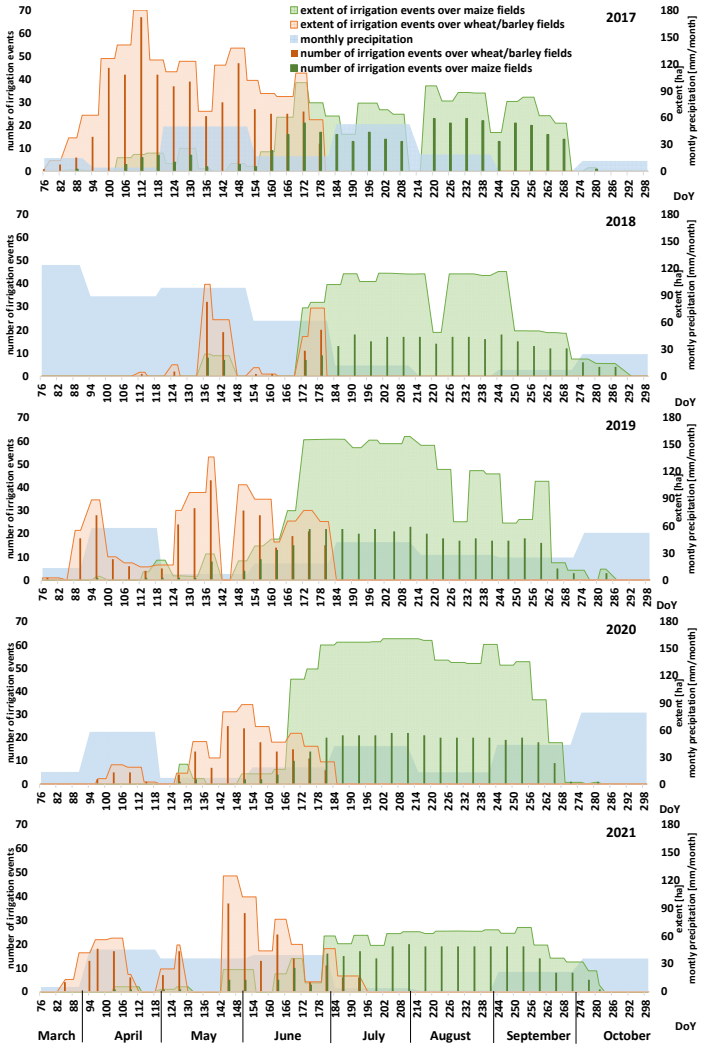


**Figure 4.** Number of irrigation events registered over the wheat and barley (red) and maize (green) fields irrigated 5 to 0 days before the S-1 passages from 2017 to 2021. Red and green shaded areas represent the extent of the irrigated fields. The monthly precipitation rate is also reported.

### *2.2. Sentinel-1 and Sentinel-2 Data*

S-1A and S-1B time series, covering the Riaza district and acquired on the ascending orbit of Relative Orbit Number (RON) 001 from 2017 to 2021, have been analyzed. The S-1 Interferometric Wide (IW) Level-1 Ground Range Detected (GRD) High Resolution (HR) product has been selected. For pre-processing, they have been calibrated, multi-looked (i.e., 4 × 4), geocoded and temporally filtered [38]. The final product is characterized by an equivalent number of looks (ENL) equal to or larger than ~80, a radiometric accuracy of ~1 dB, a pixel size of 40 m and a spatial resolution of ~100 m. From April to September, 28–30 S-1 images are available per year. In addition to S-1 data, NDVI time series derived from S-2 images have been used. The S-2 Level-2A (bottom of atmosphere reflectance) product [39] has been selected and subsequently processed to derive the NDVI index. Over Riaza, two different orbits of S-2A are available, i.e., RON 137 and 094. In total, 148 S-1 and 155 S-2 images have been coregistered and analyzed. These products are currently made available by ESA and have been downloaded from the Copernicus Open Access Hub (https://scihub.copernicus.eu/, accessed on 26 September 2022).

### *2.3. Sentinel-1 and Sentinel-2 Surface Soil Moisture Maps*

The SMOSAR code is used to transform dense time series of S-1 and S-2 acquisitions into multi-temporal SSM maps at very high resolution, i.e., ~100 m. The algorithmic development and validation have been described in Mattia et al. [40,41] and Balenzano et al. [42]. The SSM retrieval implements a short-term change detection (STCD) algorithm. It is applied to bare and vegetated surfaces dominated by soil attenuated scattering that enables good radar sensitivity to SSM throughout the growing season [43]. The land use restriction requires applying a dynamic vegetation masking to obscure those areas showing a poor radar sensitivity to SSM (i.e., areas dominated by volume scattering), before the SSM retrieval. Masking is implemented in two steps. The first one consists of using a quasi-static land cover (e.g., Climate Change Initiative (CCI) Land Cover map [44]) to mask forests, urban areas, water bodies. The second step exploits an adaptive segmentation method applied to S-1 VH colocated observations [36]. As a result, the SSM retrieval is applied only over those land surfaces dominated by soil attenuated scattering that show an adequate radar sensitivity to SSM. The contribution of S-2 NDVI data is important for retrieving SSM at a very high resolution. This is because STCD is susceptible to the occurrence of abrupt changes of the vegetation and/or soil roughness, e.g., due to tillage change [45,46], that can be wrongly interpreted as SSM changes. Such changes have a limited impact at a resolution equal to or above ~1000 m, but they usually produce significant errors at a field scale resolution. In this respect, the combined use of S-1 and S-2 data can significantly simplify the characterization of surface changes due either to vegetation or roughness conditions as described in [41]. As a result, SMOSAR can provide SSM maps either at field scale by using in input the land parcel border data wherever available or at ~100 m resolution. Both mean and standard deviation of SSM at field scale are computed and delivered.

### *2.4. Why SSM for Irrigation Identification*

The benefit of SSM maps for irrigation detection and its complementarity with respect to NDVI are first illustrated through a case study. Figure 5 (left column) shows the SSM maps, at field scale, on 22 and 4 April 2017. White areas are masked for tillage changes. Parcel borders are in black. In the right column, the NDVI maps on 22 April and 18 July 2017 are reported. In April, fields planted with winter crops show NDVI equal to or higher than 0.5, while over bare or recently planted fields NDVI is lower than 0.3. In July, NDVI follows the same pattern for summer crops.

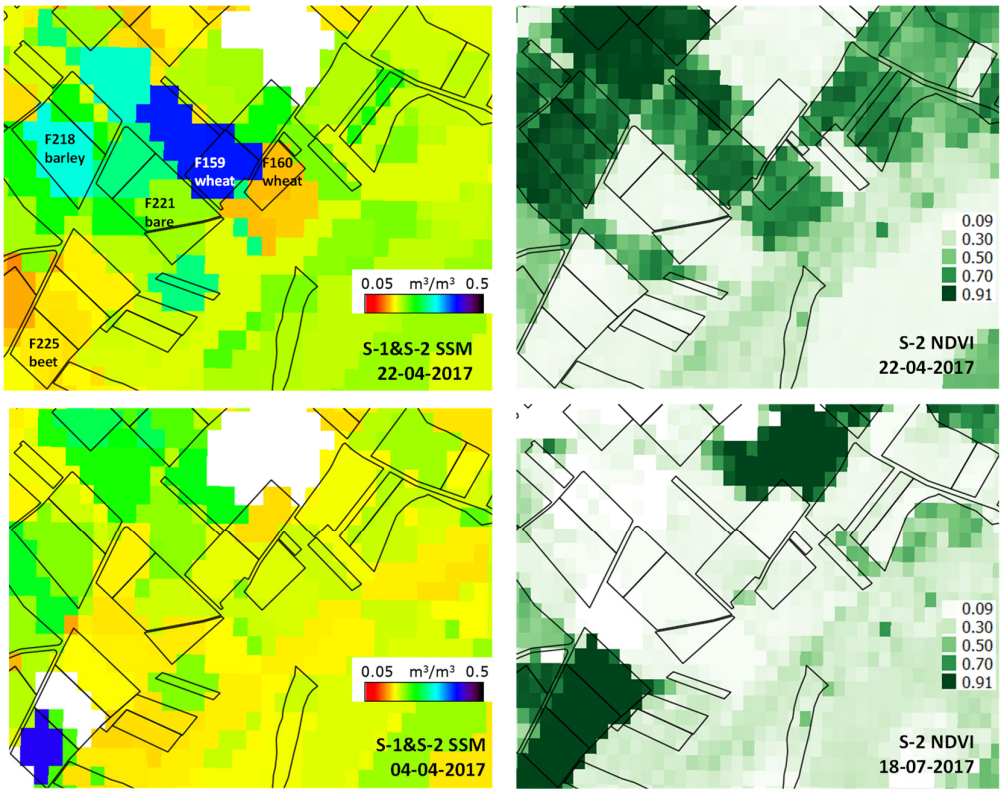


**Figure 5.** View over the Riaza irrigation district in Spain. Parcel borders are in black. **Left column**: SSM maps at field scale, derived on 22 and 4 April 2017. White areas are fields masked for tillage practice. The irrigated fields, f159, f218 and f225, show medium–high (i.e., 0.3–0.4 $m^3/m^3$) SSM levels. **Right column**: NDVI maps on 22 April and 18 July 2017.

In situ data indicate that fields f218 (winter barley) and f159 (winter wheat) were irrigated approximately one day before the S-1 passage on 22 April. In addition, field f225 (sugar beet) was irrigated approximately one day before the S-1 passage on 4 April. On the contrary, fields f160 and f221 (winter wheat) were not irrigated. Indeed, for wheat and barley, irrigation was supplemental. Conversely, for sugar beet (a summer crop), irrigation is systematically required from the early stage onward. Dark and light blue colors correspond to SSM of 0.3–0.4 $m^3/m^3$. Such high levels were sparse in the area and observed in f159 and f218 on 22 April. Therefore, they indicate the effect of irrigation that, conversely, is not evident on the NDVI map on the same date. Analogously, on 4 April, f225 showed SSM values higher than 0.3 $m^3/m^3$, consistent for a field recently irrigated. The NDVI map on April 22 confirms that f225 was almost bare. Only late in the season, e.g., on 4 July, was the greenness of the crop evident on the NDVI map.

This example provides evidence of the qualities of irrigation monitoring by SSM. First, the irrigated areas are detected well before crops appear well-developed in the NDVI maps. Second, SSM intercepts the span of irrigation events, which is not detectable by NDVI. Therefore, SSM can integrate vegetation indexes to resolve in time and space the irrigation occurrence, rather than detect the indirect effects of irrigation on crop development. Under the government's water use limitations, such a skill can be valuable, as farmers tend to abandon irrigated crops for crops, such as wheat, or permanent crops, such as vineyards, for which supplemental irrigation is sufficient.

### *2.5. Optimal Spatial Resolution for the SSM Contrast Detection*

For the detection of irrigated fields using SSM, the influence of spatial resolution turns out to be very important. As an example, Figure 6 compares SSM on 22 April 2017, at a spatial resolution of 1000 m, with that at the field scale (already shown in Figure 5) and at

100 m. Fields f159 and f218 (irrigated) and f221 (non-irrigated) are reported. Looking at the map at 1000 m, it is clear that the irrigated field f159, with a size of 2.5 ha, cannot be resolved. Considering that the average extent of the Riaza fields is 2.6 ha, the irrigation detection would require SSM information at least better than 150 m. In fact, there is often an important spatial variability of soil moisture within a single field. This is mainly because the irrigation supply usually is not uniform in space and time. For instance, Figure 6 (bottom row, left panel) depicts the SSM map on 22 April at 100 m (i.e., before averaging at field scale) and shows quite a heterogeneous irrigation pattern within the irrigated fields. In the right panel, the box plot of the SSM values shows the SSM distributions of fields f159 and f218 (irrigated) and f221 (non-irrigated). Crosses represent the SSM averages at the field scale, and the dotted lines the SSM averages at 1000 m. Averaging SSM at field scale reduces the SSM contrast. Additionally, the coarser the resolution, the smaller is the distance between averages. Under these circumstances, a pixel-wise (~40 m) segmentation of irrigated/non-irrigated areas seems more effective than that at a field scale or even at a coarser scale. Thus, the SSM maps used in this paper have been delivered at 40 m pixel size corresponding to a resolution of ~100 m. Nevertheless, the final irrigated/non-irrigated map can be subsequently aggregated at a field scale, using the parcel borders information.

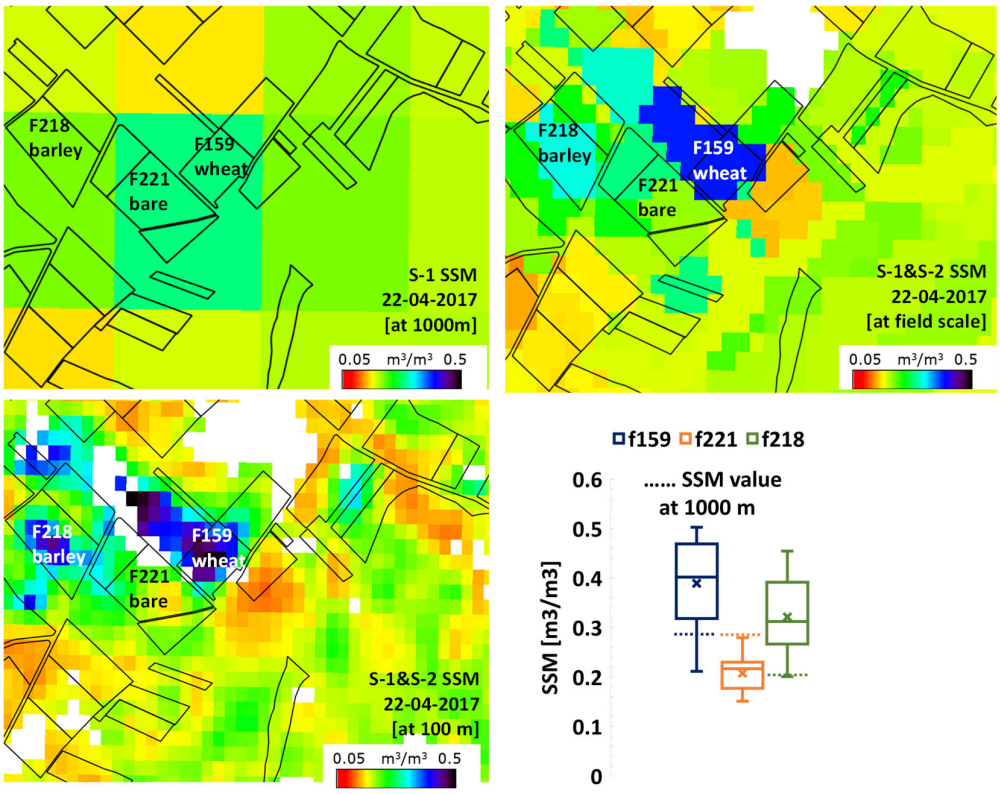


**Figure 6.** View over the Riaza irrigation district in Spain. Field borders are in black. White areas are masked for roughness or local vegetation changes. **Top row**: S-1 SSM map at 1000 m, i.e., 520 m pixel (**left panel**) and at field scale (**right panel**) on 22 April 2017 (EPSG: 4326, WGS 84). **Bottom row**: SSM map at 100 m, i.e., 40 m pixel (**left panel**). **Right panel**: box plot of the SSM distributions of the irrigated fields, f159 and f218, and non-irrigated field f221 at 100 m. Crosses represent the mean SSM value at field scale; dashed lines indicate the SSM level at 1000 m.

A second important aspect in the box plot is that the SSM dispersion within a field increases with its average, which is an intrinsic property of SSM statistics [47]. This implies that to enhance the contrast between irrigated and non-irrigated fields, it is better to adopt as a metric the distance (or the ratio) between the wettest parts of the fields rather than between the averages.

Based on this argument, the SSM contrast has been defined as:

$$C = \frac{< \mathrm{SSM}_{75Q} >_{\mathrm{irr}}}{< \mathrm{SSM}_{75Q} >_{\mathrm{no\ irr}}}, \quad (1)$$

where < > indicates the spatial average over the irrigated or non-irrigated pixels. The SSM values higher than the third quartile (75Q) have been identified and averaged.

Only fields including a spatial average over at least 10% of the total pixels have been considered. The total number of wheat and barley irrigated fields ranges from 94 in 2018 to 119 in 2017, while the total number of maize irrigated fields ranges from 23 in 2018 to 31 in 2017.

## 3. Results and Discussion

The potential of the contrast index defined above to identify the irrigated areas during the crop growing season and the main disturbing factors are identified. Figure 7 depicts the logical flow of data in the analysis. EO inputs are S-1 and S-2 images that are transformed by SMOSAR into SSM maps at very high resolution. Then, the analysis is supported by ancillary data, such as irrigation management, meteorological data and parcel borders. The SSM contrast is derived according to (1). Results are finally analyzed to characterize the main factors which may jeopardize the irrigation detection.

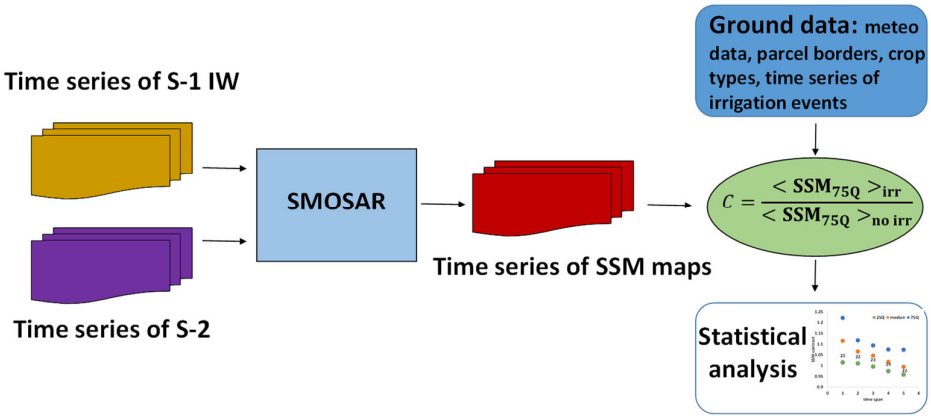


**Figure 7.** Data flow diagram.

### *3.1. Causes of Incertitude in Mapping Irrigated Areas*

#### 3.1.1. Effect of Irrigation Timing

The effect on the contrast of the time span ($TS$) between the S-1 acquisition date and the irrigation date is analyzed for wheat and barley fields. It is worth recalling that, in the context of this study, a field is considered irrigated if it received a water supply at most 5 days before the S-1 passage. Therefore, for each S-1 acquisition, from 2017 to 2021 and from April to June, the irrigated fields can be classified based on their $TS$ distance (i.e., $0 \leq TS \leq 5$). For the homogeneity of the sample, only the S-1 dates when at least four fields were irrigated have been considered. Then, for each irrigation date the contrast between irrigated and non-irrigated fields has been computed according to (1) and labeled with the appropriate $TS$. Subsequently, the distribution of the SSM contrast as a function of $TS$ has been investigated. Figure 8 shows the first and third quartile of the SSM contrast distribution, as well as the median, for each $TS$. The number of the S-1 acquisitions dates per $TS$ is also reported. In general, percentiles decrease from 1 to 5 $TS$. Up to $TS$ = 3, for approximately 75% of the total SSM maps, the irrigated fields show a contrast higher than 1 ($C > 1$). In principle, they can all be discriminated from non-irrigated fields. At $TS$ = 1, the highest contrast is achieved. It ranges between 1.11 and 1.22 for 50% of the total SSM maps. Conversely, for $TS$ = 5, the contrast is less than 1 for 50% of the total SSM maps. It is

noted that, in Figure 8, all the S-1 passages for which precipitation events occurred in the previous 24 h have been disregarded. The rationale is illustrated in the next section.

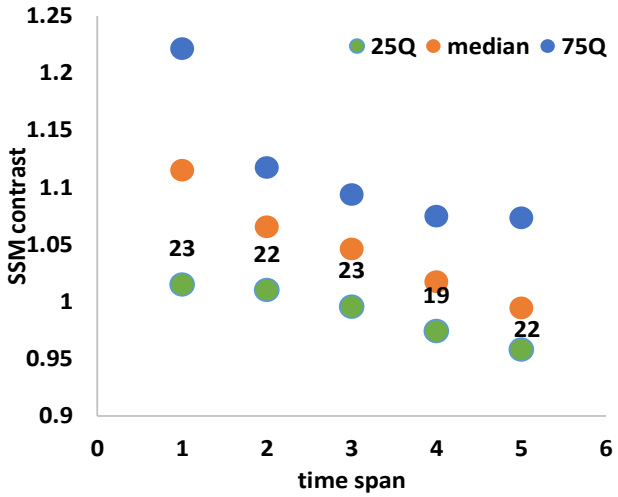


**Figure 8.** First quartile (25Q, green points), median (orange points) and third quartile (75Q, blue points) of the SSM contrast between irrigated and non-irrigated wheat/barley fields as a function of the time span (*TS*) between the irrigation events and the S-1 passages. The number of the S-1 acquisition dates is also reported.

### 3.1.2. Effect of Precipitation

The impact of precipitation on the SSM contrast is summarized in Figure 9. It is the same as Figure 8 but only for the S-1 passages preceded by precipitation events. Clearly, precipitations close to the S-1 passage reduce the SSM contrast, smoothing the difference between the SSM level of the irrigated and non-irrigated fields. Whenever the irrigation occurred, the median of the contrast is approximately 1, regardless of *TS*. Therefore, Figure 9 conveys the message that the presence of localized precipitation events largely affects the identification of irrigated fields.

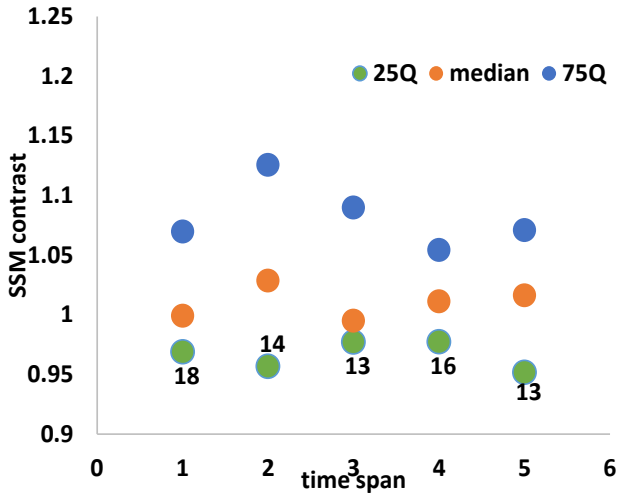


**Figure 9.** As for Figure 8, but for the S-1 acquisition dates when precipitation occurred within 24 h.

### 3.1.3. Effect of Water Supply

It is now instructive to address the dependence of SSM contrast on water supply. Data reported in Figure 8, at *TS* = 1, have been separated into two groups. The first one concerns fields where the water supply was between 1 and 15 mm, while the second shows those between 15 and 45 mm. Figure 10 shows the first and third quartile of the SSM contrast

distribution, as well as the median, for each group. In general, the SSM contrast increases with the water supply. However, in the case of medium–low irrigation, for approximately 50% of the total cases, the SSM contrast is less than 1.

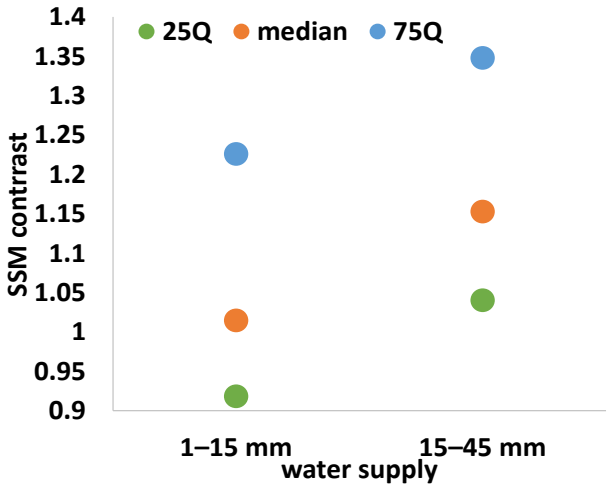


**Figure 10.** First quartile (25Q, green points), median (orange points) and third quartile (75Q, blue points) of the SSM contrast as a function of water supply in case of $TS = 1$ of Figure 8.

#### 3.1.4. Effect of Vegetation Cover

Finally, the case of irrigated maize fields is discussed. The procedure to compute the contrast as a function of $TS$ is the same as for the winter crops. The only difference is that for maize, almost all the fields were irrigated on any date. Therefore, as a reference for non-irrigated areas, the harvested wheat and barley fields (i.e., NDVI $< 0.3$) have been considered.

Figure 11 reports the SSM contrast distribution as a function of $TS$. It can be noted that for $TS = 1$ ($TS > 1$), approximately 75% (50%) of the total S-1 passages show an SSM contrast higher (less) than 1. Comparing Figures 8 and 11, two main variations can be noted. First, the SSM contrast of maize fields is less sensitive than wheat to $TS$. This is likely because maize fields are mainly irrigated from July–August. In this period, the reference evapotranspiration rate reaches the highest values, i.e., approximately 5.5 mm/w on average (see green shaded area in Figure 12), which corresponds to 6.6 mm/w crop evapotranspiration for maize in the mid-season according to the FAO56 method (https://www.fao.org/3/x0490e/x0490e0b.htm, accessed on 26 September 2022), thus facilitating the drying out process after irrigation. Second, the SSM contrast in the case of maize fields is generally lower than the SSM contrast of wheat/barley fields. Reasonably, this is due to the reduced sensitivity of the S-1 signal to SSM of maize, particularly in its mature phase. The effect is investigated in Figure 12, which reports the temporal behavior of the average and standard deviation of SSM observed over irrigated maize (at $TS = 1$) and non-irrigated wheat/barley fields in 2021. The behavior of the SSM contrast is also reported (purple circles). The purple dashed line is the linear fit of temporal contrast. It indicates a decrease in time with the development of the crop, i.e., from emergence of the plants to the mature stage (i.e., NDVI $> 0.6$).

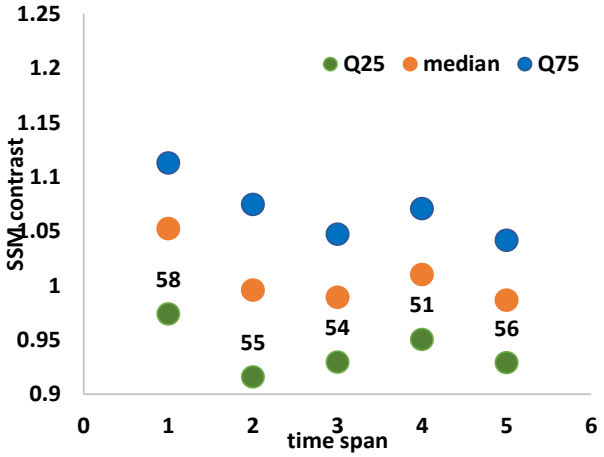


**Figure 11.** As for Figure 8, but for maize fields.

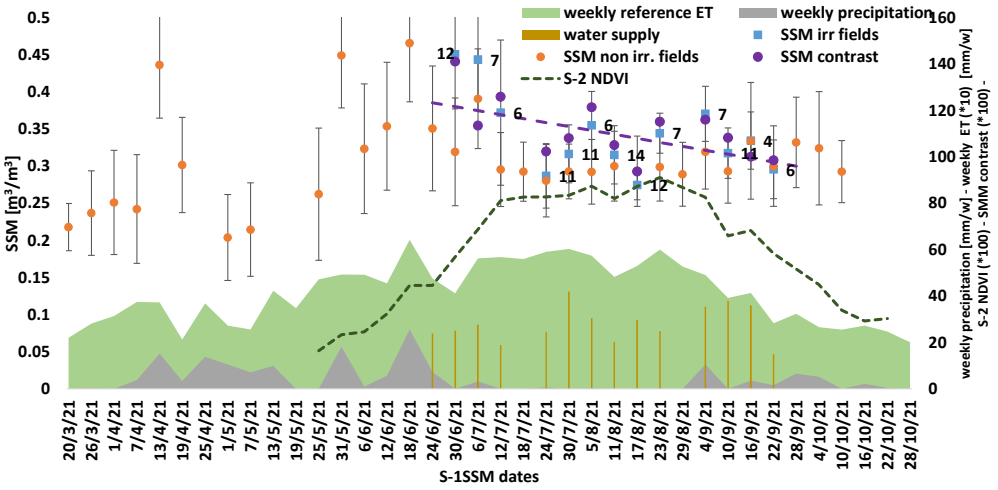


**Figure 12.** Temporal behavior of average SSM of maize irrigated (blue squares) within 1 day before the S-1 passages and non-irrigated wheat/barley (orange circles) fields in 2021. Bars refer to the inter-field variability. The number of maize fields irrigated is in black. Time series of SSM contrast (purple circles scaled by 100) and their linear fit (purple dashed line) are on the secondary axis. Weekly precipitation and reference evapotranspiration (ET) rate (scaled by 10) are reported in gray and green shaded areas on the secondary axis, too, as well as the S-2 NDVI (dashed green line, scaled by 100).

### *3.2. Perspectives for Mapping Irrigated Areas by S-1 and S-2 SSM*

A first outcome of the analysis is that the presence of localized precipitation events reduces the contrast of irrigated and non-irrigated areas, thus hampering the irrigated areas' detection in a time window somewhere colocated with the precipitations. In the same vein, for example, Bazzi et al. [32] recently observed over a test site in France a reduced separability between irrigated and non-irrigated fields by using S-1 and S-2 data during years with high precipitation. Therefore, automatic detection of precipitation patterns is needed as a preliminary step for mapping irrigated areas. Algorithms mapping precipitation fields already exist (e.g., [48,49]) and could be integrated.

Another crucial factor affecting SSM irrigation detection is the temporal resolution of the EO observations. For the analyzed data set, a three-day revisit is necessary to capture 75% of the total cases. However, one-day revisit would significantly increase the observed SSM contrast. This result is also in line with the findings of Le Page et al. [50] and Bazzi et al. [51]. The studies analyzed the effect of the S-1 temporal resolution on the capability of irrigation detection over 4 and 46 irrigated maize and grassland plots,

respectively, in France. They concluded that an irrigation event over low vegetation cover (NDVI < 0.7) could be detected until three days after the irrigation occurrence. Beyond three days, the possibility of detecting irrigation events decreases due to the drying out of the soil, a few days after the irrigation event. In this respect, the next generation of the S-1 constellation (S-1 NG) and the forthcoming EU L-band Radar Observation System for Europe (ROSE-L) system [52] should approach a one-day revisit. Additionally, they will provide complementarity between microwave frequencies that can overcome some of the shortcomings observed over well-developed crops [53], such as the loss of S-1 sensitivity to SSM over maize.

Currently, the use of vegetation indexes to detect irrigated summer crops, in a mature stage, may seem more robust than SSM. A promising scenario encompasses SAR in tandem with optical data. SSM can support an early detection of the irrigation events, while optical indexes are more reliable late in the growing season. The continuous monitoring of the irrigated areas can be accumulated per season to produce a time-dependent extent of irrigated areas, which is crucial for water management models.

In summary, the benefit of integrating multi-frequency and multi-platform EO data to detect irrigated areas is a continuous monitoring that can produce accurate time-dependent extents of actual irrigated areas. This improved information serves a more efficient irrigation management. In particular, the capability of SAR data to identify supplemental irrigation can support the objective of improving water withdrawal estimates as recommended by the new European Common Agricultural Policy (CAP) monitoring.

## 4. Conclusions

This study investigated the retrieval of irrigation land use, at the district scale, by SSM at ~100 m resolution, derived from S-1 and S-2 observations. A large and well-documented data set, acquired over the Riaza irrigation district (Spain), has provided the experimental basis to characterize the SSM contrast between irrigated and non-irrigated fields. Results indicate that the contrast generally decreases as *TS* (time span between the irrigation event and the S-1 acquisition) increases. Approximately 75% of irrigated fields show a contrast larger than 1 for *TS* equal to or less than three days. Therefore, they can be isolated. Additionally, the level of the SSM contrast depends on the amount of water supplied per field and on the meteorological conditions. Moreover, it is influenced by the sensitivity of SAR data to SSM underneath winter and summer crops. In particular, for maize a decline in the contrast during the mature phase has been observed. In this respect, an integrative use of SSM and vegetation indexes can provide timely information on the extent of irrigated areas during the entire growing season. To consolidate the results, the analysis will be extended to other agricultural areas, e.g., in southern Italy.

**Author Contributions:** Conceptualization, A.B. and F.M.; methodology, A.B. and A.D.; software, G.S., R.G. and D.P.; formal analysis, A.B.; resources, D.N.G. and V.P.G.; data curation, F.P.L.; writing—original draft preparation, A.B. and F.M.; writing—review and editing, all; visualization, O.O. All authors have read and agreed to the published version of the manuscript.

**Funding:** This research was supported by the project "Use of multi-frequency SAR data for AGRIculture" (SARAGRI), funded by the Italian Space Agency (ASI) under contract N. 2021-6-U.0 and by the Horizon 2020 Research and Innovation Program of the European Union, through the project "Sentinels Synergy for Agriculture (SENSAGRI)" (Grant Agreement n° 730074).

**Institutional Review Board Statement:** Not applicable.

**Informed Consent Statement:** Not applicable.

**Data Availability Statement:** The data presented in this study are available on request from the corresponding author.

**Acknowledgments:** The authors would like to thank Maria Mottola for her administrative and technical support.

**Conflicts of Interest:** The authors declare no conflict of interest.

## References


1. United Stations Environment Programme. Mediterranean Action Plan. UNEP/MED WG.502/6 2021. Available online: https://www.rac-spa.org/publications (accessed on 26 September 2022).
2. Tramblay, Y.; Koutroulis, A.; Samaniego, L.; Vicente-Serrano, S.M.; Volaire, F.; Boone, A.; Le Page, M.; Llasat, M.C.; Albergel, C.; Burak, S.; et al. Challenges for Drought Assessment in the Mediterranean Region under Future Climate Scenarios. *Earth-Sci. Rev.* **2020**, *210*, 103348. [CrossRef]
3. IPCC. *Climate Change 2022: Impacts, Adaptation, and Vulnerability. Contribution of Working Group II to the Sixth Assessment Report of the Intergovernmental Panel on Climate Change*; Pörtner, H.-O., Roberts, D.C., Tignor, M., Poloczanska, E.S., Mintenbeck, K., Alegría, A., Craig, M., Langsdorf, S., Löschke, S., Möller, V., et al., Eds.; Cambridge University Press: Cambridge, UK; New York, NY, USA, 2022. [CrossRef]
4. Food and Agriculture Organization (FAO). *The State of Food and Agriculture 2020. Overcoming water Challenges in Agriculture*; FAO: Rome, Italy, 2020; ISBN 978-92-5-133441-6.
5. Ferguson, C.R.; Pan, M.; Oki, T. The Effect of Global Warming on Future Water Availability: CMIP5 Synthesis. *Water Resour. Res.* **2018**, *54*, 7791–7819. [CrossRef]
6. Islam, N.; Winkel, J. Climate Change and Social Inequality. DESA Working Paper No. 152, ST/ESA/2017/DWP/152. 2017. Available online: https://www.un.org/development/desa/publications/working-paper/wp152 (accessed on 26 September 2022).
7. Rosa, L. Adapting agriculture to climate change via sustainable irrigation: Biophysical potentials and feedbacks. *Environ. Res. Lett.* **2022**, *17*, 063008. [CrossRef]
8. McNally, A.; McCartney, S.; Ruane, A.C.; Mladenova, I.E.; Whitcraft, A.K.; Becker-Reshef, I.; Bolten, J.D.; Peters-Lidard, C.D.; Rosenzweig, C.; Uz, S.S. Hydrologic and Agricultural Earth Observations and Modeling for the Water-Food Nexus. *Front. Environ. Sci.* **2019**, *7*, 23. [CrossRef]
9. Zajac, Z.; Gomez, O.; Gelati, E.; van der Velde, M.; Bassu, S.; Ceglar, A.; Chukaliev, O.; Panarello, L.; Koeble, R.; van den Berg, M.; et al. Estimation of spatial distribution of irrigated crop areas in Europe for large-scale modelling applications. *Agric. Water Manag.* **2022**, *266*, 107527. [CrossRef]
10. Puy, A.; Borgonovo, E.; Lo Piano, S.; Levin, S.A.; Saltelli, A. Irrigated areas drive irrigation water withdrawals. *Nat. Commun.* **2021**, *12*, 4525. [CrossRef]
11. Paredes-Gómez, V.; Gutiérrez, A.; Del Blanco, V.; Nafría, D.A. A Methodological Approach for Irrigation Detection in the Frame of Common Agricultural Policy Checks by Monitoring. *Agronomy* **2020**, *10*, 867. [CrossRef]
12. Meier, J.; Zabel, F.; Mauser, W. A global approach to estimate irrigated areas–a comparison between different data and statistics. *Hydrol. Earth Syst Sci.* **2018**, *22*, 1119–1133. [CrossRef]
13. Puy, A.; Sheikholeslami, R.; Gupta, H.V.; Hall, J.W.; Lankford, B.; Lo Piano, S.; Meier, J.; Pappenberger, F.; Porporato, A.; Vico, G.; et al. The delusive accuracy of global irrigation water withdrawal estimates. *Nat. Commun.* **2022**, *13*, 3183. [CrossRef]
14. Massari, C.; Modanesi, S.; Dari, J.; Gruber, A.; De Lannoy, G.J.M.; Girotto, M.; Quintana-Seguí, P. A review of irrigation information retrievals from space and their utility for users. *Remote Sens.* **2021**, *13*, 4112. [CrossRef]
15. Karthikeyan, L.; Chawla, I.; Mishra, A.K. A review of remote sensing applications in agriculture for food security: Crop growth and yield, irrigation, and crop losses. *J. Hydrol.* **2020**, *586*, 124905. [CrossRef]
16. Ha, W.; Gowda, P.H.; Howell, T.A. A review of downscaling methods for remote sensing-based irrigation management: Part I. *Irrig. Sci.* **2013**, *31*, 831–850. [CrossRef]
17. Ha, W.; Gowda, P.H.; Howell, T.A. A review of potential image fusion methods for remote sensing-based irrigation management: Part II. *Irrig. Sci.* **2013**, *31*, 851–869. [CrossRef]
18. Pervez, M.; Budde, M.; Rowland, J. Mapping irrigated areas in Afghanistan over the past decade using MODIS NDVI. *Remote Sens. Environ.* **2014**, *149*, 155–165. [CrossRef]
19. Ambika, A.K.; Wardlow, B.; Mishra, V. Remotely sensed high resolution irrigated area mapping in India for 2000 to 2015. *Sci. Data* **2016**, *3*, 160118. [CrossRef]
20. Gumma, M.K.; Thenkabail, P.S.; Hideto, F.; Nelson, A.; Dheeravath, V.; Busia, D.; Rala, A. Mapping irrigated areas of Ghana using fusion of 30 m and 250 m resolution remote-sensing data. *Remote Sens.* **2011**, *3*, 816–835. [CrossRef]
21. Xie, Y.; Lark, T.J.; Brown, J.F.; Gibbs, H.K. Mapping irrigated cropland extent across the conterminous United States at 30 m resolution using a semi-automatic training approach on Google Earth Engine. *ISPRS J. Photogramm. Remote Sens.* **2019**, *155*, 136–149. [CrossRef]
22. Lawston, P.M.; Santanello, J.A., Jr.; Kumar, S.V. Irrigation signals detected from SMAP soil moisture retrievals. *Geophys. Res. Lett.* **2017**, *44*, 11–860. [CrossRef]
23. Brocca, L.; Tarpanelli, A.; Filippucci, P.; Dorigo, W.; Zaussinger, F.; Gruber, A.; Fernández-Prieto, D. How much water is used for irrigation? A new approach exploiting coarse resolution satellite soil moisture products. *Int. J. Appl. Earth Obs. Geoinf.* **2018**, *73*, 752–766. [CrossRef]
24. Dari, J.; Quintana-Seguí, P.; Escorihuela, M.J.; Stefan, V.; Brocca, L.; Morbidelli, R. Detecting and mapping irrigated areas in a Mediterranean environment by using remote sensing soil moisture and a land surface model. *J. Hydrol.* **2021**, *596*, 126129. [CrossRef]
25. El Hajj, M.; Baghdadi, N.; Zribi, M.; Bazzi, H. Synergic use of Sentinel-1 and Sentinel-2 images for operational soil moisture mapping at high spatial resolution over agricultural areas. *Remote Sens.* **2017**, *9*, 1292. [CrossRef]

26. Bauer-Marschallinger, B.; Freeman, V.; Cao, S.; Paulik, C.; Schaufler, S.; Stachl, T.; Modanesi, S.; Massari, C.; Ciabatta, L.; Brocca, L.; et al. Toward global soil moisture monitoring with Sentinel-1: Harnessing assets and overcoming obstacles. *IEEE Trans. Geosci. Remote Sens.* **2018**, *57*, 520–539. [CrossRef]
27. Balenzano, A.; Mattia, F.; Satalino, G.; Lovergine, F.P.; Palmisano, D.; Peng, J.; Marzahn, P.; Wegmüller, U.; Cartus, O.; Dąbrowska-Zielińska, K.; et al. Sentinel-1 soil moisture at 1 km resolution: A validation study. *Remote Sens. Environ.* **2021**, *263*, 112554. [CrossRef]
28. Gao, Q.; Zribi, M.; Escorihuela, M.J.; Baghdadi, N.; Segui, P.Q. Irrigation mapping using Sentinel-1 time series at field scale. *Remote Sens.* **2018**, *10*, 1495. [CrossRef]
29. Bousbih, S.; Zribi, M.; El Hajj, M.; Baghdadi, N.; Lili-Chabaane, Z.; Gao, Q.; Fanise, P. Soil moisture and irrigation mapping in A semi-arid region, based on the synergetic use of Sentinel-1 and Sentinel-2 data. *Remote Sens.* **2018**, *10*, 1953. [CrossRef]
30. Elwan, E.; Le Page, M.; Jarlan, L.; Baghdadi, N.; Brocca, L.; Modanesi, S.; Dari, J.; Quintana Seguí, P.; Zribi, M. Irrigation mapping on two contrasted climatic contexts using Sentinel-1 and Sentinel-2 data. *Water* **2022**, *14*, 804. [CrossRef]
31. Dari, J.; Brocca, L.; Quintana-Seguí, P.; Casadei, S.; Escorihuela, M.J.; Stefan, V.; Morbidelli, R. Double-scale analysis on the detectability of irrigation signals from remote sensing soil moisture over an area with complex topography in central Italy. *Adv. Water Resour.* **2022**, *161*, 104130. [CrossRef]
32. Bazzi, H.; Baghdadi, N.; Amin, G.; Fayad, I.; Zribi, M.; Demarez, V.; Belhouchette, H. An Operational Framework for Mapping Irrigated Areas at Plot Scale Using Sentinel-1 and Sentinel-2 Data. *Remote Sens.* **2021**, *13*, 2584. [CrossRef]
33. Ali, E.; Cramer, W.; Carnicer, J.; Georgopoulou, E.; Hilmi, N.J.M.; le Cozannet, G.; Lionello, P. Cross-Chapter Paper 4: Mediterranean Region. In *Climate Change 2022: Impacts, Adaptation and Vulnerability. Contribution of Working Group II to the Sixth Assessment Report of the Intergovernmental Panel on Climate Change*; Pörtner, H.-O., Roberts, D.C., Tignor, M., Poloczanska, E.S., Mintenbeck, K., Alegría, A., Craig, M., Langsdorf, S., Löschke, S., Möller, V., et al., Eds.; Cambridge University Press: Cambridge, UK; New York, NY, USA, 2022; pp. 2233–2272. [CrossRef]
34. Ouellette, J.D.; Johnson, J.T.; Balenzano, A.; Mattia, F.; Satalino, G.; Kim, S.B.; Dunbar, R.S.; Colliander, A.; Cosh, M.H.; Caldwell, T.G.; et al. A time-series approach to estimating soil moisture from vegetated surfaces using L-band radar backscatter. *IEEE Trans. Geosci. Remote Sens.* **2017**, *55*, 3186–3193. [CrossRef]
35. Iacobellis, V.; Gioia, A.; Milella, P.; Satalino, G.; Balenzano, A.; Mattia, F. Inter-comparison of hydrological model simulations with time series of SAR-derived soil moisture maps. *Eur. J. Remote Sens.* **2013**, *46*, 739–757. [CrossRef]
36. Satalino, G.; Balenzano, A.; Mattia, F.; Davidson, M.W.J. C-band SAR data for mapping crops dominated by surface or volume scattering. *IEEE Geosci. Remote Sens. Lett.* **2014**, *11*, 384–388. [CrossRef]
37. Palmisano, D.; Mattia, F.; Balenzano, A.; Satalino, G.; Pierdicca, N.; Guarnieri, A.V.M. Sentinel-1 sensitivity to soil moisture at high incidence angle and the impact on retrieval over seasonal crops. *IEEE Trans. Geosci. Remote Sens.* **2021**, *59*, 7308–7321. [CrossRef]
38. Quegan, S.; Yu, J.J. Filtering of multichannel SAR images. *IEEE Trans. Geosci. Remote Sens.* **2001**, *39*, 2373–2379. [CrossRef]
39. Sentinel-2 MSI User Guide Product Type: Level-2A. April 2019. Available online: https://sentinel.esa.int/web/sentinel/user-guides/sentinel-2-msi/product-types/level-2a (accessed on 26 September 2022).
40. Mattia, F.; Balenzano, A.; Satalino, G.; Lovergine, F.; Peng, J.; Wegmuller, U.; Cartus, O.; Davidson, M.W.J.; Kim, S.; Johnson, J.; et al. Sentinel-1 & Sentinel-2 for SOIL Moisture Retrieval at Field Scale. In Proceedings of the IGARSS 2018—2018 IEEE International Geoscience and Remote Sensing Symposium, Valencia, Spain, 22–27 July 2018; pp. 6143–6146. [CrossRef]
41. Mattia, F.; Satalino, G.; Balenzano, A.; Lovergine, F.P.; D'Addabbo, A. Final SSM Algorithm Theoretical Basis Document. EU SARAGRI Project, Deliverable 3.8. 2019. Available online: https://leoipl.uv.es/sensagri/ftp/DELIVERABLES/WP3/SENSAGRI_D3_8_v10.pdf (accessed on 26 September 2022).
42. Paredes Gómez, V.; Balenzano, A.; Mattia, F.; Satalino, G.; Lovergine, F.P.; D'Addabbo, A.; Nafría García, D. Second Validation of Surface Soil Moisture Maps. EU SARAGRI Project, Deliverable 7.16. 2019. Available online: https://leoipl.uv.es/sensagri/ftp/DELIVERABLES/WP7/SENSAGRI_D7.16_v10.pdf (accessed on 26 September 2022).
43. Balenzano, A.; Mattia, F.; Satalino, G.; Davidson, M. Dense temporal series of C-and L-band SAR data for soil moisture retrieval over agricultural crops. *IEEE J. Sel. Top. Appl. Earth Obs. Remote Sens.* **2011**, *4*, 439–450. [CrossRef]
44. Product User Guide. 2017. ESA Land Cover CCI v2.0. Tech. Rep. Available online: https://www.esa-landcover-cci.org/?q=node/199 (accessed on 26 September 2022).
45. Mattia, F. Coherent and incoherent scattering from tilled soil surfaces. *Waves Random Complex Media* **2011**, *21*, 278–300. [CrossRef]
46. Mattia, F.; Le Toan, T.; Davidson, M. An analytical, numerical, and experimental study of backscattering from multiscale soil surfaces. *Radio Sci.* **2001**, *36*, 119–135. [CrossRef]
47. Famiglietti, J.S.; Ryu, D.; Berg, A.A.; Rodell, M.; Jackson, T.J. Field observations of soil moisture variability across scales. *Water Resour. Res.* **2008**, *44*, W01423. [CrossRef]
48. Rysman, J.F.; Verrier, S.; Lemaître, Y.; Moreau, E. Space-time variability of the rainfall over the western Mediterranean region: A statistical analysis. *J. Geophys. Res. Atmos.* **2013**, *118*, 8448–8459. [CrossRef]
49. Chiaravalloti, F.; Brocca, L.; Procopio, A.; Massari, C.; Gabriele, S. Assessment of GPM and SM2RAIN-ASCAT rainfall products over complex terrain in southern Italy. *Atmos. Res.* **2018**, *206*, 64–74. [CrossRef]
50. Le Page, M.; Jarlan, L.; El Hajj, M.M.; Zribi, M.; Baghdadi, N.; Boone, A. Potential for the Detection of Irrigation Events on Maize Plots Using Sentinel-1 Soil Moisture Products. *Remote Sens.* **2020**, *12*, 1621. [CrossRef]

51. Bazzi, H.; Baghdadi, N.; Fayad, I.; Charron, F.; Zribi, M.; Belhouchette, H. Irrigation Events Detection over Intensively Irrigated Grassland Plots Using Sentinel-1 Data. *Remote Sens.* **2020**, *12*, 4058. [CrossRef]
52. Davidson, M.; Iannini, L.; Torres, R.; Geudtner, D. New perspectives for applications and services provided by future spaceborne SAR missions at the European Space Agency. In Proceedings of the International Geoscience and Remote Sensing Symposium (IGARSS2022), Kuala Lumpur, Malaysia, 17–22 July 2022; pp. 4720–4723.
53. Bazzi, H.; Baghdadi, N.; Charron, F.; Zribi, M. Comparative Analysis of the Sensitivity of SAR Data in C and L Bands for the Detection of Irrigation Events. *Remote Sens.* **2022**, *14*, 2312. [CrossRef]